RSC Advances

PAPER

View Article Online
View Journal | View Issue

Open Access Article. Published on 23 December 2020. Downloaded on 3/29/2026 8:09:53 AM.
This article is licensed under a Creative Commons Attribution-NonCommercial 3.0 Unported Licence.

Check for updates

Cite this: *RSC Adv.*, 2021, **11**, 268

Recovery of valuable metals from mixed spent lithium-ion batteries by multi-step directional precipitation†

Xuan Yang,[b] Yingjie Zhang,[ab] Qi Meng,*[a] Peng Dong,*[a] Peichao Ning[b] and Qingxiang Li[c]

Received 1st November 2020
Accepted 13th December 2020

DOI: 10.1039/d0ra09297e

rsc.li/rsc-advances

The novel strategy of multi-step directional precipitation is proposed for recovering valuable metals from the leachate of cathode material obtained by mechanical disassembly from mixed spent lithium-ion batteries. Based on thermodynamics and directional precipitation, Mn^{2+} is selectively precipitated under conditions of MRNM (molar ratio of $(NH_4)_2S_2O_8$ to Mn^{2+}) = 3, pH = 5.5 and 80 °C for 90 min. Ni^{2+} was then selectively precipitated using $C_4H_8N_2O_2$ under conditions of pH = 6, MRCN (molar ratio of $C_4H_8N_2O_2$ to Ni^{2+}) = 2, 30 °C and 20 min. Then, the pH was adjusted to 10 to precipitate Co^{2+} as $Co(OH)_2$. Finally, Li^+ was recovered by Na_2CO_3 at 90 °C. The precipitation rates of Mn, Ni, Co, and Li reached 99.5%, 99.6%, 99.2% and 90%, respectively. The precipitation products with high purity can be used as raw materials for industrial production based on characterization. The economical and efficient recovery process can be applied in industrialized large-scale recycling of spent lithium-ion batteries.

1. Introduction

Lithium-ion batteries (LIBs) have been widely used in portable electronic equipment and new energy vehicles because of their high energy density, low self-discharge rate, and light weight, *etc.*[1,2] With the large consumption and growing demand for LIBs, a large number of spent LIBs will be generated due to their limited average life of 2–4 years.[3,4] Spent LIBs contain heavy metals, organic chemicals, plastics, *etc.*, which will cause great harm to the environment.[5,6] Meanwhile, spent LIBs contain valuable metals of Ni, Co, Mn, Li, *etc.*, which will cause the squandering of resources without reasonable recycling.[7,8] Therefore, the recycling of spent LIBs is necessary for protecting the environment and saving resources.[9,10]

The recycling methods of spent LIBs mainly include pyrometallurgy processes[11–13] and hydrometallurgy processes.[14–16] Compared with the pyrometallurgy process,[17] the hydrometallurgy process is widely used due to its advantages of mild operating conditions, high metal recovery, *etc.*[18,19] Leaching is an important step in hydrometallurgy.[20,21] Some researchers have used organic acids as leachates due to its mild and environment friendly conditions, such as tartaric acid,[22] citric acid,[23] oxalic acid,[24] *etc.* However, the organic acids of leaching process seem low leaching efficiency and unsatisfied for following process.[25] Inorganic acid is often used in leaching process because of its cheap price and high leaching efficiency, including HCl,[26,27] HNO_3,[28] H_2SO_4,[29–31] *etc.* Therefore, the inorganic acid is common reagent for leaching process, which seems be fully developed.

Separation of valuable metals from leachate after leaching has gained more attention, mainly including solvent extraction and chemical precipitation. The selection of extractant is the research focus of solvent extraction. There are a lot of researches on solvent extraction. Wang *et al.* used D2EHPA to extract copper and manganese.[32] Jha *et al.* used Cyanex 272 to extract Co and extraction rate reaches 99.9%.[33] Suzuki *et al.* used PC-88A/TOA mixed extractant to separate Co from leachate, the extraction rate was more than 98%.[34] The solvent extraction methods can obtain high purity products, but it has disadvantages of high toxicity and high cost.

In order to reduce process cost, the chemical precipitation method with simplify process flow and improve process integrity have also been reported. Chen *et al.* used oxalic acid to separate Co from leach solution and the precipitation rate reached 98%.[9] Wang *et al.* used $KMnO_4$ to separate Mn from leaching solution, the precipitation rate reached 98%.[26] Barik *et al.* used Na_2CO_3 to separate Li from leachate and the precipitation rate reached 91%.[35] The precipitation method has the advantages of simple operation and low cost. However, co-precipitation is easy to occur in the precipitation process,

[a]*National and Local Joint Engineering Laboratory for Lithium-ion Batteries and Materials Preparation Technology, Key Laboratory of Advanced Battery Materials of Yunnan Province, Faculty of Metallurgy and Energy Engineering, Kunming University of Science and Technology, Kunming 650093, China. E-mail: mengqi315117@126.com; dongpeng2001@126.com*

[b]*Faculty of Materials Science and Engineering, Kunming University of Science and Technology, Kunming 650093, China*

[c]*Shenzhen Zhongjin Lingnan Technology Co., Ltd., Shenzhen 518118, China*

† Electronic supplementary information (ESI) available. See DOI: 10.1039/d0ra09297e

© 2021 The Author(s). Published by the Royal Society of Chemistry

Open Access Article. Published on 23 December 2020. Downloaded on 3/29/2026 8:09:53 AM.
This article is licensed under a Creative Commons Attribution-NonCommercial 3.0 Unported Licence.

which reduces the purity of the product. Therefore, it is very important to choose a suitable precipitant agent.

Moreover, most recycle research are reported on a single kind of spent LIBs, which was pretreated by manual disassembly with low efficiency and dangerous. Therefore, more effective recycling strategy, such as mechanical disassembly, should be developed for recycling of mixed spent LIBs. However, the related research has been rarely reported.

A novel recovery process of multi-step directional precipitation was proposed to recover the valuable metals from mixed spent LIBs. Based on pretreatment process, the leachate was obtained from mixed spent LIBs with mechanical disassembly, leaching and impurities removal step. Then, the selective precipitants were used for step by step separation of Mn, Ni, Co and Li. The effect of variables was investigated to obtain directional separation optimal conditions. To analyze selective precipitation process, the reaction mechanism and precipitation products was characterized by XRD, SEM, FTIR. To further analysis the economy of process, the material balance, energy balance and waste management in the whole process was analyzed. The whole process is green, efficient and economical with high purity precipitation products and without waste liquid, which can provide a new idea for the industrial application of high efficiency and economic recovery of mixed spent LIBs.

2. Experimental section

2.1 Materials and reagents

The mixed spent LIBs used here were collected from BYD Technology Co., Ltd. The disassembled products were obtained by mechanical disassembly. The specific process of mechanical disassembly is shown in Fig. S1.† The disassembled products were analyzed by X-ray Diffraction (XRD) and thermogravimetric analysis-differential scanning calorimetry (TG-DSC). All reagents used here were analytical grade and solutions were prepared with deionized water.

2.2 Pretreatment process

10 g of disassembled products were calcined at an optimal temperature based on analysis of TG-DSC to obtain spent residues. The contents of metals in spent residues were measured by inductively coupled plasma optical emission spectrometer (ICP-OES). The results are shown in Table S1.†

In order to improve the separation efficiency of Ni, Co, Mn and Li, impurities such as Al, Cu and Fe should be removed before separation step. The spent residues were immersed in 3 mol L^{-1} NaOH solution at 60 °C for 2 h, and then washed three times with deionized water and filtered to obtain spent cathode materials. The spent cathode materials were leached in 3 mol L^{-1} H_2SO_4 under conditions of 3 vol% H_2O_2, solid–liquid ratio of 20 g L^{-1}, 80 °C for 1 h to obtain leachate. Subsequently, iron was used for remove copper in the leachate under the condition of pH = 1.5 and ultrasound at 30 °C for 20 minutes. After filtration, the pH of leachate was adjusted to 3.5 to remove Fe at 90 °C. Finally, the leachate was obtained and analyzed by ICP-OES. The results are shown in Table S2.†

2.3 Separation process of valuable metals

The multi-step directional precipitation method was used to recover valuable metals from the leachate. A certain amount of $(NH_4)_2S_2O_8$ powders were added to a certain volume of leachate in a 250 ml three neck flask and stirring rate was controlled at 300 rpm. The effects of pH value, temperature, molar ratio of $(NH_4)_2S_2O_8$ to Mn^{2+} (MRNM) and time on the reaction were studied. Under the optimal conditions of Mn recovery, the remaining leachate was treated to obtain the solution enriched with Ni, Co, Li and products of Mn. The same experimental operations were used for recovery of Ni and Co. The Ni from the filtrate was precipitated by $C_4H_8N_2O_2$ (DMG). The effects of pH, molar ratio of $C_4H_8N_2O_2$ to Ni^{2+}(MRCN), temperature and reaction time were studied to obtain optimal conditions. NaOH was added to the filtrate to remove cobalt after the recovery of Ni under the optimum conditions. The pH, temperature and reaction time of the solution are controlled to obtain optimal conditions for cobalt separation. Subsequently, a certain amount of Na_2CO_3 was added, and the reaction temperature was adjusted. Lithium was recovered as Li_2CO_3 by high-temperature filtration. The content changes of Mn, Ni, Co, Li in the separation process were shown in Table S3.†

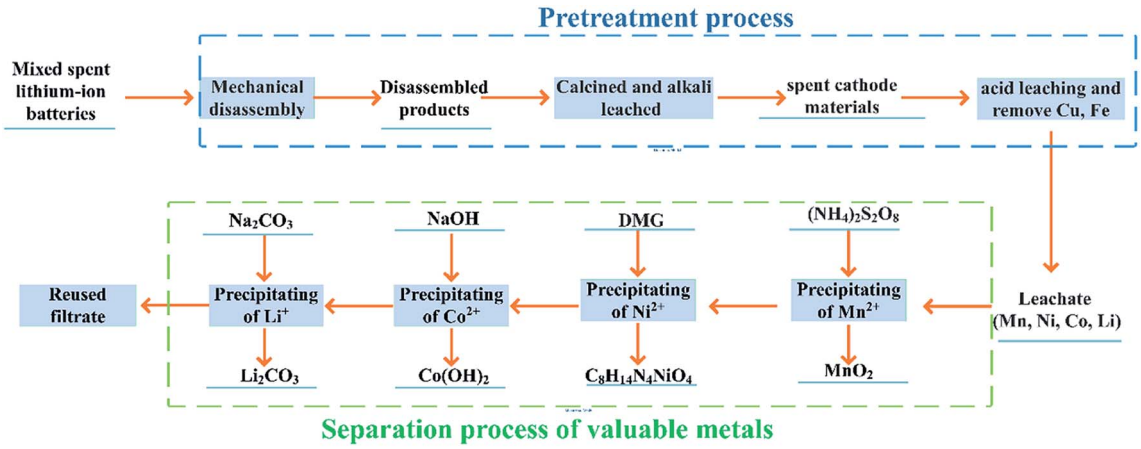

Fig. 1 Overall flow path of the recovery process of metal values from mixed spent LIBs.

Open Access Article. Published on 23 December 2020. Downloaded on 3/29/2026 8:09:53 AM.
This article is licensed under a Creative Commons Attribution-NonCommercial 3.0 Unported Licence.

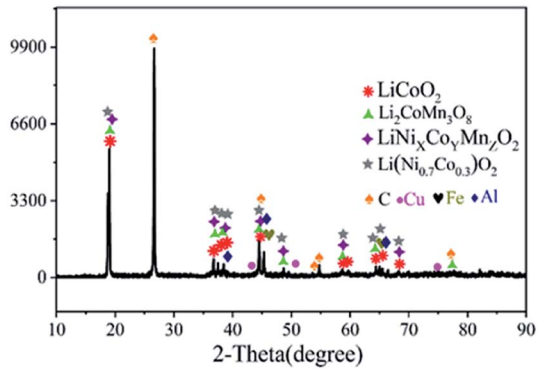

Fig. 2 Image of XRD pattern of spent cathode materials before calcination.

The precipitation rates of metals were calculated according to eqn (1):

$$P = \frac{V_b C_b - V_a C_a}{V_a C_a} \times 100\% \quad (1)$$

where P is the metal precipitation rate; C_a and C_b are the metal ion concentrations in the solution before and after precipitation; V_a and V_b are the solution volumes before and after precipitation.

Finally, the recovery process for the recycling of mixed spent LIBs was proposed in Fig. 1. After obtaining the optimal conditions for recovery Mn, Ni, Co, and Li, a scale-up experiment was conducted. 100 g of disassembled products were subjected by recovery process and economic evaluation was carried out.

2.4 Analytical methods

The metal concentration in the solution was measured by ICP-OES (PerkinElmer Optima 8000).

A pH meter (PHS-25, 2000) was used for real-time pH monitoring and adjustment. During the experiment, the pH was adjusted using 1 mol L^{-1} H_2SO_4 and 1 mol L^{-1} NaOH solution. A pH meter (PHS-25, 2000) was used for real-time pH monitoring and adjustment. During the experiment, the pH was adjusted using 1 mol L^{-1} H_2SO_4 and 1 mol L^{-1} NaOH solution. The composition of the precipitated product was detected and determined by X-ray diffractometer (XRD, Rigaku Japan). Sample morphology and elemental composition were obtained by scanning electron microscopy (SEM, TESCAN VEGA3, CZE) coupled with energy-dispersive X-ray spectroscopy (EDS). FTIR spectrometer (Nicolet Is10) was used to detect the functional groups of $C_8H_{14}N_4NiO_4$ to verifying the precipitated product.

3. Results and discussion

3.1 Pretreatment process

The compositions of the disassembled products were characterized by XRD. As shown in Fig. 2, $LiCoO_2$, $LiNi_xCo_yMn_zO_2$, $Li(Ni_{0.7}Co_{0.3})O_2$, $Li_2CoMn_3O_8$ and other phases exist in the cathode powders. The phases of $LiCoO_2$, $LiNi_xCo_yMn_zO_2$, $Li(Ni_{0.7}Co_{0.3})O_2$ indicated that the mechanically pulverized spent batteries contain both lithium cobaltite batteries, ternary batteries and possibly other types of batteries. The phase of $Li_2CoMn_3O_8$ may be generated from the heat of mechanical crushing, which causes various cathode materials to mix and react to form a mixed phase. In addition, the cathode powders contain C, Al, Fe, and Cu. C is mainly derived from the anode materials and acetylene black of the LIBs. Al, Cu and Fe are derived from the positive electrode current collectors, negative electrode current collectors and the case of the spent LIBs, respectively.

Fig. 3(a) shows the TG/DSC pattern of the disassembled products. As shown in the Fig. 3(a), the endothermic peak at 0–250 °C corresponds to the loss of crystal water. The exothermic peak at 250–350 °C corresponds to the combustion of the battery separator (PP). The endothermic peak at 350–450 °C corresponds to the PVDF decomposition. The exothermic peak at 550–760 °C corresponds to the combustion of carbon. In order to remove the non-metallic impurities completely, the calcination temperature was selected at 800 °C.

Fig. 3(b) shows the XRD diffraction pattern of the disassembled products calcined at 800 °C. As shown in Fig. 3(b), the Al, Fe, and Cu impurities are oxidized to form corresponding oxides while the peak of C disappears. It was attributed to the combustion decomposition of C at a high temperature of 800 °C. Moreover, the phases of $LiNiO_2$ and $Li_4Mn_5O_{12}$ appeared in the Fig. 3(b). This is because the structure of the

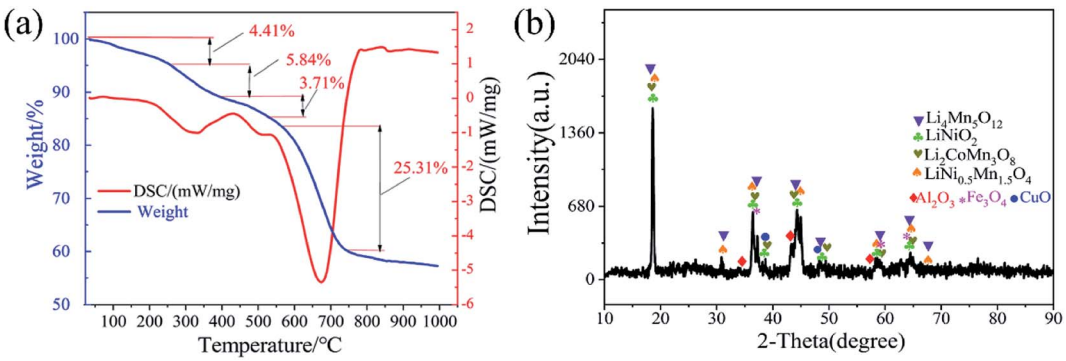

Fig. 3 (a) Images of TG/DSC pattern of spent cathode materials; (b) image of XRD pattern of disassembled products after calcined.

 © 2021 The Author(s). Published by the Royal Society of Chemistry

Open Access Article. Published on 23 December 2020. Downloaded on 3/29/2026 8:09:53 AM.
This article is licensed under a Creative Commons Attribution-NonCommercial 3.0 Unported Licence.

cathode material has been restored to a certain extent, which proves that the spent cathode powders are made up of cathode materials of various spent LIBs. Meanwhile, as shown in Table S1,† the disassembled products contain Al, Fe and Cu, which must be removed before subsequent valuable metal separation process steps. After the impurities of Al, Cu and Fe were removed, the contents of each metal in the leachate were shown in Table S2.† As shown in Table S2,† the contents of Al, Cu and Fe are 0.002 g L^{-1}, 0.002 g L^{-1} and 0.004 g L^{-1}, respectively. The impurities are basically removed effectively, which provides good conditions for the subsequent separation process. Impurities were effectively removed which indicated that the leachate can be used for subsequent study on the separation of valuable metals.

3.2 Analysis of Mn separation process

3.2.1 Reaction mechanism. Based on the basic thermodynamic data, the *E*–pH diagram of for the Mn–H_2O system at an ion concentration of 1 mol L^{-1} were obtained. As shown in Fig. S2,† with the increases of potential, Mn^{2+} in the solution may be oxidized to generate a mixed product of Mn_xO_y including MnO_2, Mn_3O_4 and MnOOH. These phases can exist stably in the aqueous solution, so the proper oxidant can be selected to recover Mn^{2+} from the leachate. In previous reports, $KMnO_4$ was used to oxidize Mn^{2+} to form oxide.[26] However, $KMnO_4$ can introduce K^+ into the leaching solution and is dangerous in operation, other suitable oxidants should be considered. Table S4† shows the possible electrode reactions and corresponding standard electrode potentials in the leaching solution. As shown in Table S4,† the reduction potential of $S_2O_8^{2-}$ is much higher than the reduction potential of Mn^{2+}. Therefore, $S_2O_8^{2-}$ can be used as a suitable oxidant. In order to reduce the introduction of impurity ions, $(NH_4)_2S_2O_8$ instead of $Na_2S_2O_8$ was used as Mn precipitation separator. The reaction potential of $S_2O_8^{2-}$ is also higher than that of Ni^{2+} and Co^{2+}, and Co^{2+} and Ni^{2+} will also be oxidized while Mn^{2+} is oxidized. Therefore, appropriate precipitation conditions should be selected to reduce the reaction.

3.2.2 Optimal condition of Mn precipitation. In order to obtain the best precipitation rate, four variables in precipitation process were investigated. Fig. 4 shows the effects of MRNM, reaction pH, temperature and time on the precipitation rate of valuable metals. As shown in Fig. 4(a), the precipitation rate of Mn^{2+} reached 99.5% at MRNM = 3. Meanwhile, the precipitation rate of other elements is still lower than 5%. The precipitation rate of Mn almost no longer increased but instead the precipitation rate of Co increases with increasing MRNM from 3 to 3.5. The optimum condition is therefore MRNM = 3. With the increase of temperature, the precipitation rate of Mn has increased significantly. The precipitation rate reached 99.2% at 80 °C. As the temperature increases from 80 °C to 90 °C, the precipitation rate did not increase significantly. With the increase of pH, the precipitation rate of Mn increased continuously and reached the highest value at pH = 5.5. The precipitation rate of Mn^{2+} decreased and the precipitation rate of Co increased significantly when the pH increased to 6.5, which caused by the small amount of $Co(OH)_2$ has been formed at pH

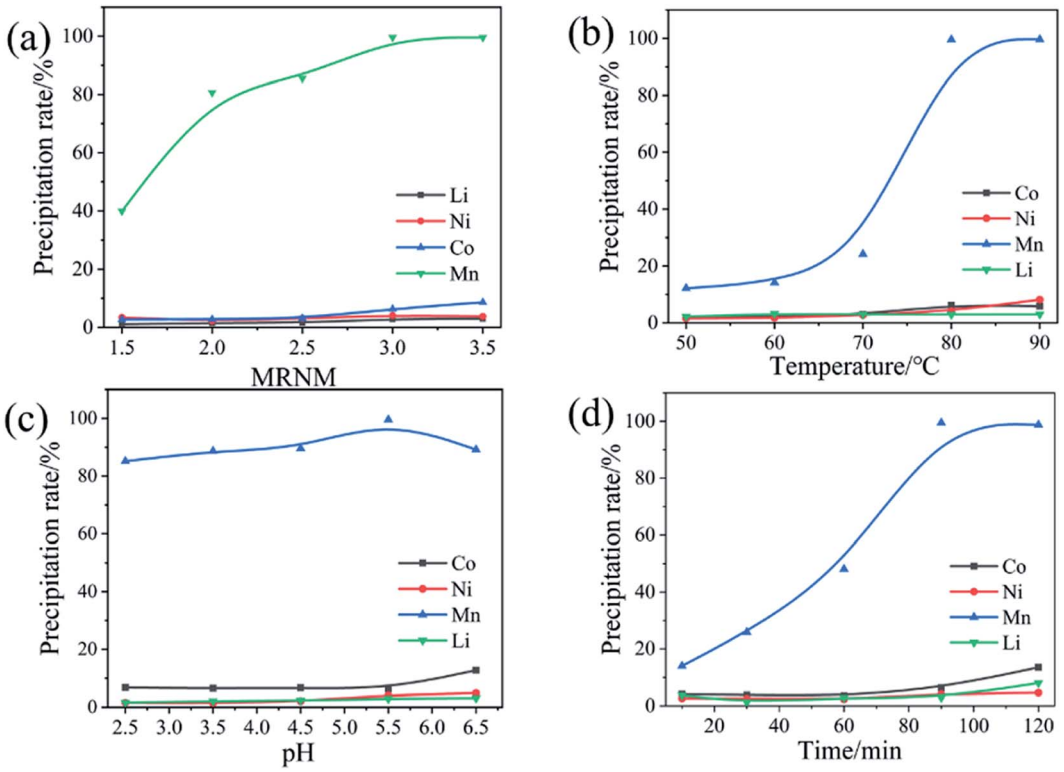

Fig. 4 Effect of different experimental conditions on precipitation rate. (a) MRNM (80 °C, pH = 5.5, 90 min, 300 rpm); (b) temperature (MRNM = 3, pH = 5.5, 90 min, 300 rpm); (c) pH (80 °C, MRNM = 3, 90 min, 300 rpm); (d) time (80 °C, pH = 5.5, MRNM = 3, 300 rpm).

Open Access Article. Published on 23 December 2020. Downloaded on 3/29/2026 8:09:53 AM.
This article is licensed under a Creative Commons Attribution-NonCommercial 3.0 Unported Licence.

= 6.5. Equilibrium pH of 5.5 is therefore suitable for the precipitation process. With the increase of time, the precipitation rate increased significantly, and the precipitation rate reached the highest value at 90 minutes. When the reaction time increased from 90 minutes to 120 minutes, the precipitation rate of Mn basically unchanged, but the precipitation rates of Co, Li increased to 12.5% and 8.0%, respectively. In summary, under the optimal conditions of MRNM = 3, 80 °C, pH = 5.5, 90 min, the precipitation rate of Mn, Ni, Co and Li reached 99.5%, 3.0%, 4.0%, and 2.9%, respectively. Fig. S3† shows recovery rate of various metals in precipitation of Mn. As shown in Fig. S3,† a small amount of Co and Ni were precipitated out, which is due to Co^{2+} and Ni^{2+} can be oxidized to form $Co(OH)_3$ and NiO_2.

3.2.3 Products of Mn precipitation. Fig. 5 is XRD pattern and SEM-EDS image of the precipitated products after adding $(NH_4)_2S_2O_8$ to the leaching solution. The XRD pattern in Fig. 5 shows that Mn^{2+} in the leachate is oxidized and precipitated in the form of a mixture of MnO_2 and Mn_2O_3. Meanwhile, it can be seen from the EDS images of the precipitated products that the main elements in the precipitated products are Mn and O, which indicates that the precipitated products are mainly composed of manganese oxide. The above results show that Mn^{2+} can be effectively separated from other metal ions and the purity of product is 96.5%. The precipitation reaction takes place as follows:

$$Mn^{2+} + S_2O_8^{2-} + 2H_2O = MnO_2 + 2SO_4^{2-} + 4H^+ \quad (2)$$

$$2Mn^{2+} + S_2O_8^{2-} + 3H_2O = Mn_2O_3 + 2SO_4^{2-} + 6H^+ \quad (3)$$

3.3 Ni separation process

3.3.1 Reaction mechanism. $C_4H_8N_2O_2$ (DMG) can form a water-insoluble chelate with Ni and does not react with other ions.[36] Therefore, dimethylglyoxime is selected to separate Ni and the precipitation reaction can be expressed as follows:

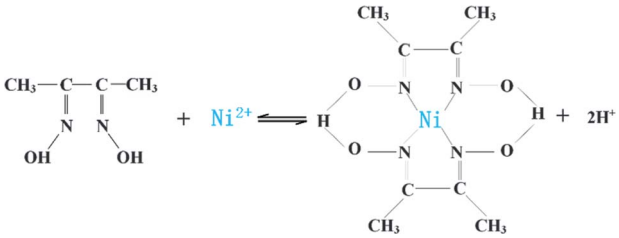

3.3.2 Optimal condition of Ni precipitation. The effects of MRCN, temperature, pH, and time on the precipitation rates of Li, Ni, and Co were shown in Fig. 6. The precipitation rate of Ni^{2+} increases significantly with the MRCN increased. Meanwhile, the precipitation rate of other metal ions has almost no changed and keeps a low state. The effect of temperature on the chelation between DMG and Ni^{2+} was not significant. The precipitation rate of Ni^{2+} has basically reached the maximum value at 30 °C, and the effect of increasing temperature on the

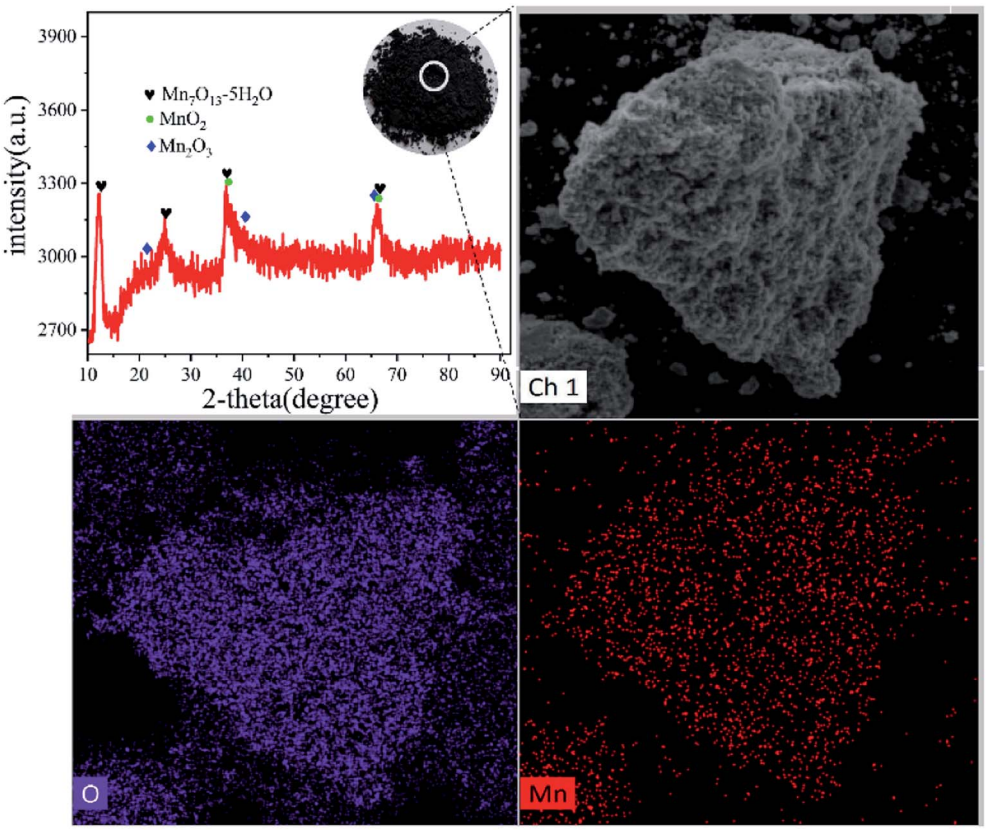

Fig. 5 Images of XRD pattern and SEM-EDS of products of Mn precipitation.

 © 2021 The Author(s). Published by the Royal Society of Chemistry

Open Access Article. Published on 23 December 2020. Downloaded on 3/29/2026 8:09:53 AM.
This article is licensed under a Creative Commons Attribution-NonCommercial 3.0 Unported Licence.

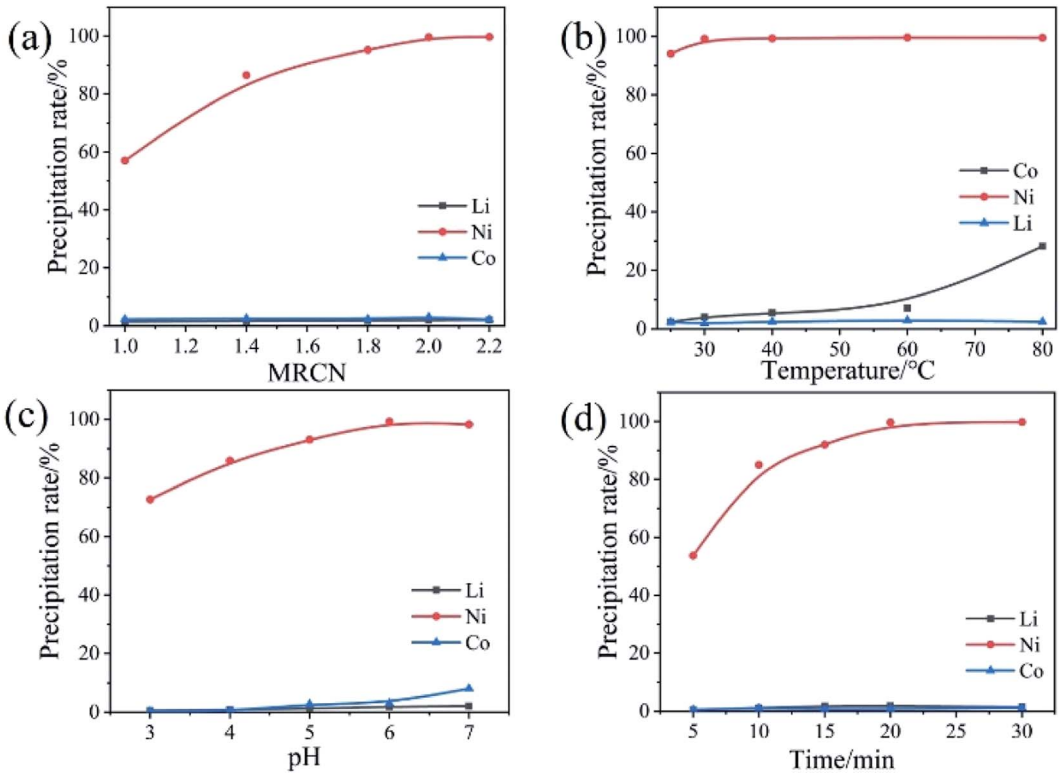

Fig. 6 Effect of different experimental conditions on precipitation rate. (a) MRCN (30 °C, pH = 6, 20 min, 300 rpm); (b) temperature (MRCN = 2, pH = 6, 90 min, 300 rpm); (c) pH (30 °C, MRCN = 2, 20 min, 300 rpm); (d) time (30 °C, pH = 6, MRCN = 2, 300 rpm).

precipitation rate was minimal. Meanwhile, the precipitation rate of Co^{2+} was increasing with the increase of temperature, which is due to the formation of cobalt oxime complexes between Co^{2+} and DMG. With the increase of pH, the precipitation rate of Ni^{2+} raised significantly. This is because the reaction will generate H^+ while generating $C_8H_{14}N_4NiO_4$. According to the principle of chemical equilibrium movement, the increase of pH value will push the reaction forward and make the reaction more thorough. However, the precipitation rate of Co^{2+} increases at pH = 7, which is due to the formation of $Co(OH)_2$ under these conditions. The precipitation reaction proceeded very quickly and rose to a maximum in the first 20 minutes. After that, the precipitation rate of Ni^{2+} hardly changed with time. In summary, the precipitation rate of Ni, Co and Li is 99.6%, 2.1% and 1.9% under the optimal conditions of MRCN = 2, 20 min, 30 °C, pH = 6, respectively. Fig. S4† shows recovery rate of Ni, Co and Li during Ni precipitation process. As shown in Fig. S4,† Ni is effectively separated, Co and Li are retained, which guarantees the high purity of the product.

3.3.3 Products of Ni precipitation. Fig. 7(a) shows an infrared spectrum image of the precipitated product. The vibration peak at 3447.28 cm^{-1} corresponds to the stretching vibration peak of the O–H bond; the vibration peak at 1571.88 cm^{-1} corresponds to the stretching vibration peak of

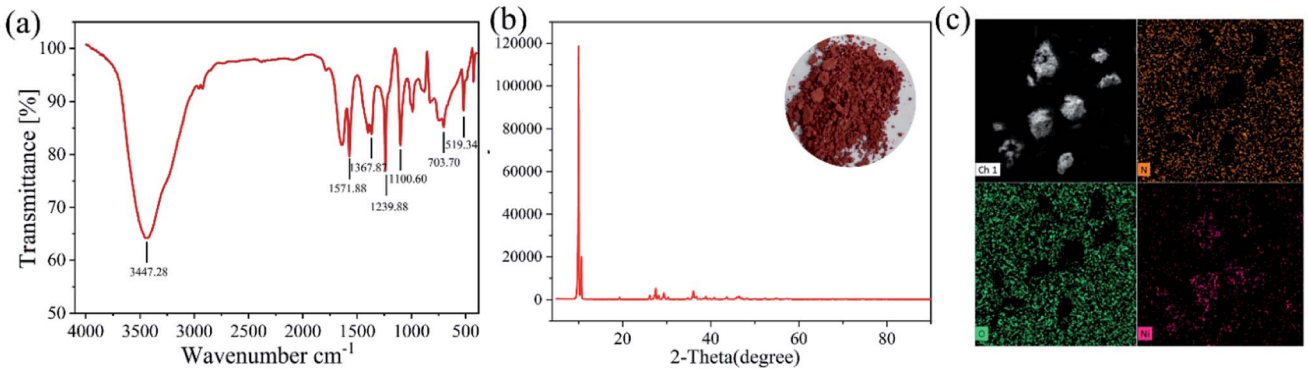

Fig. 7 (a) Images of infrared spectra of the precipitate product after treating with DMG; (b) images of XRD pattern of the precipitate product after treating with DMG; (c) images of EDS of the precipitate product after treating with DMG.

Open Access Article. Published on 23 December 2020. Downloaded on 3/29/2026 8:09:53 AM.
This article is licensed under a Creative Commons Attribution-NonCommercial 3.0 Unported Licence.

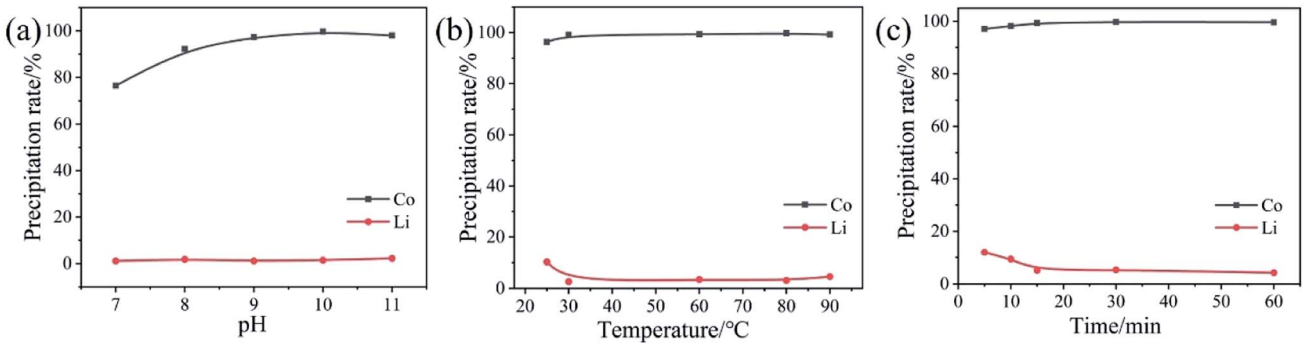

Fig. 8 Effect of different experimental conditions on precipitation rate. (a) pH (30 °C, 20 min, 300 rpm); (b) temperature (pH = 10, 20 min, 300 rpm); (c) time (30 °C, pH = 10, 300 rpm).

the C=N double bond; the vibration peak at 1367.87 cm^{-1} corresponds to N–OH bending vibration peaks. 1239.88 cm^{-1} and 1100.30 cm^{-1} correspond to the N–O antisymmetric and symmetric stretching vibration peaks caused by the coordination of N–OH groups with Ni^{2+}, respectively; 730.7 cm^{-1} and 519.34 cm^{-1} are all correspond to the absorption peak of N–Ni bond. The XRD diffraction pattern of the precipitated product is shown in Fig. 7(b). XRD pattern indicates that relatively pure precipitation product of DMG–Ni could be obtained. The EDS image of the precipitated product is shown in Fig. 7(c). The main elements on the precipitated surface are O, N and Ni. Besides, the purity of the product is 98.3% obtained by ICP, which indicated that Ni^{2+} could be effectively recovered from leachate by selective precipitation.

3.4 Analysis of Co separation process

3.4.1 Reaction mechanism. Fig. S5† shows the *E*–pH diagram based on basic thermodynamic data for the Co–H_2O system at an ion concentration of 1 mol L^{-1}. According to Fig. S5,† as the potential increases, Co^{2+} in the solution. With

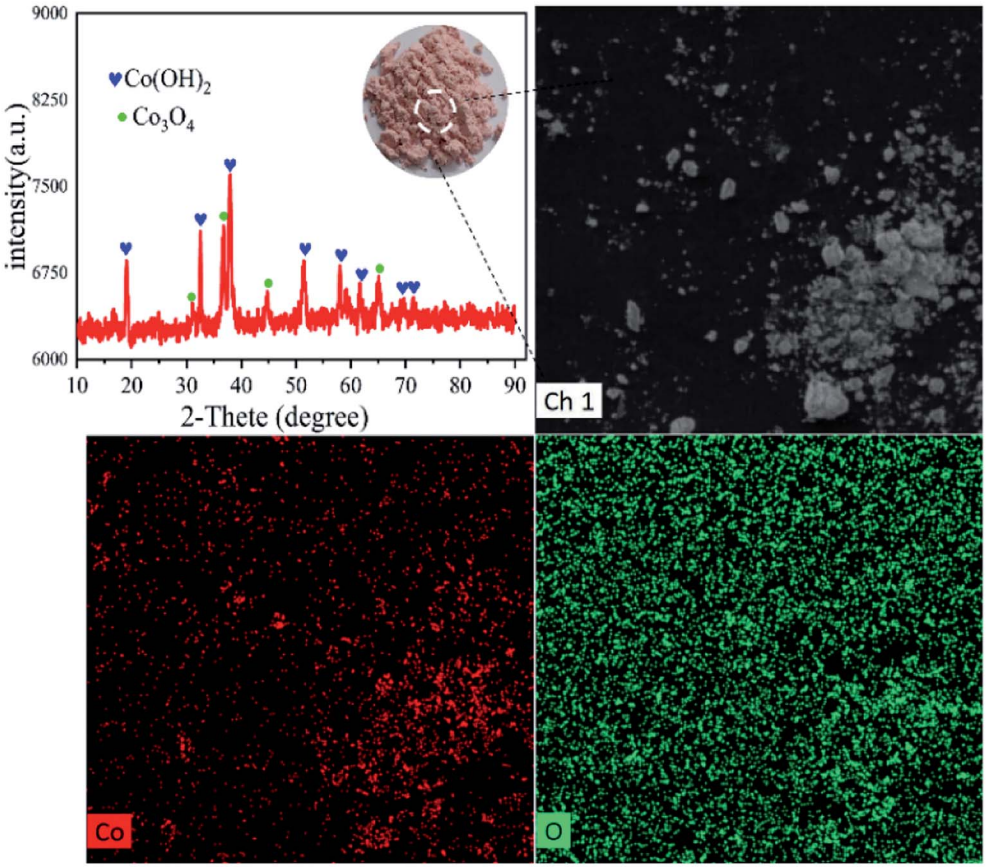

Fig. 9 Images of XRD and EDS pattern of the precipitate product after treating with NaOH.

 © 2021 The Author(s). Published by the Royal Society of Chemistry

Open Access Article. Published on 23 December 2020. Downloaded on 3/29/2026 8:09:53 AM.
This article is licensed under a Creative Commons Attribution-NonCommercial 3.0 Unported Licence.

the increase of the potential under basic conditions, Co^{2+} can form $Co(OH)_2$, which are hardly soluble in water. This indicates that adjusting the pH of the solution to alkaline can separate Co^{2+} from Li^+. According to the above analysis, Co^{2+} can be separated from the leachate in the appropriate pH. Besides, the solubility of LiOH in water is about 12.8 g/100 ml, indicating the co-precipitation of Co and Li is almost impossible. Therefore, it is economical and effective to adjust the pH with sodium hydroxide solution to separate of Co^{2+}. The precipitation reaction takes place as follows:

$$Co^{2+} + 2OH^- = Co(OH)_2 \quad (4)$$

3.4.2 Optimal condition of Co precipitation. Fig. 8(a) shows the precipitation rates of Co and Li at different pH. As shown in the Fig. 8(a), the precipitation rate of Co^{2+} increased significantly with the increase of pH, which reached a maximum at pH = 10. With the increase of pH, there was no significant difference in precipitation rate. This is because the reaction has been basically completed at pH = 10, and too much OH^- has no significance. The effect of temperature on the progress of the reaction was not obvious. When the temperature reached 30 °C, the precipitation rate was already close to the maximum. The precipitation rate has basically unchanged when the temperature was continuously increased. As shown in the Fig. 8(c), the reaction proceeded very quickly and reached its maximum at first 15 min. However, if the reaction time is too short, the loss rate of Li^+ will increase, which was attributed to the excessively short reaction time causing the generated $Co(OH)_2$ to be loosely porous and entrain some Li^+. In conclusion, pH = 10, 15 min and reaction temperature of 30 °C would be the optimized experimental conditions, under which 99.2% of Co could be recovered.

3.4.3 Products of Co precipitation. As shown in the Fig. 9, the precipitated products are mainly $Co(OH)_2$ and a small amount of Co_3O_4 formed by oxidation. It can be observed that relatively pure precipitated products could be obtained, which indicated that Co^{2+} can be efficiently separated from the solution. As shown in the EDS diagram, the main elements in the precipitated products are O and Co. Fig. S6† shows precipitation rate of Co and Li. As shown in the Fig. S6,† Co is precipitated efficiently while only a very small amount of Li has been lost. The purity of the product is 97.4%, which indicated that the product with high purity.

3.5 Recovery of lithium

Li^+ was precipitated from the leachate by Na_2CO_3. The temperature of the leachate was raised to 90 °C, and Na_2CO_3 was added to the leaching solution in an amount twice that of Li^+. About 90% of Li^+ was recovered as Li_2CO_3 with a purity of over 99%. In order to minimize the loss of lithium, the entrained impurity ions must be quickly filtered at high temperature and washed with hot deionized water (close to 100 °C). Fig. S7† shows an XRD pattern of Na_2CO_3 treatment and precipitation obtained. As shown in Fig. S7,† the precipitated

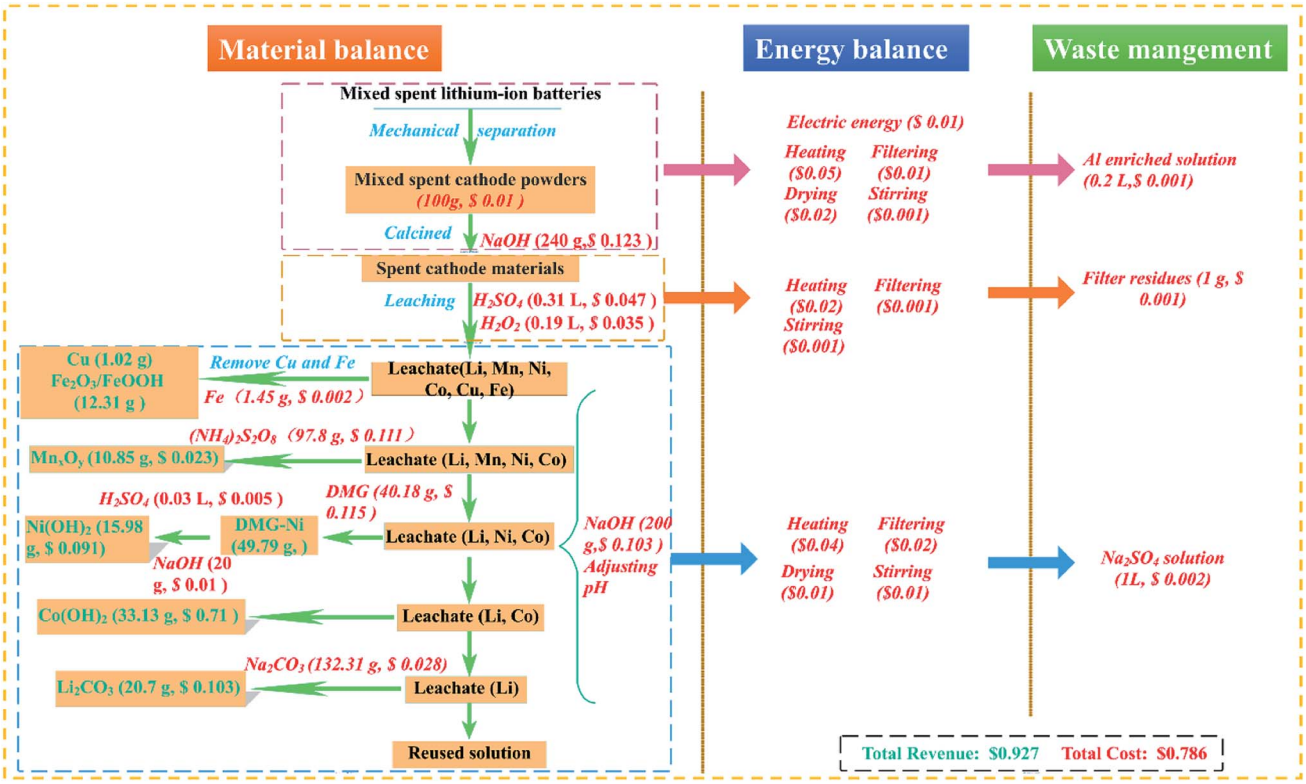

Fig. 10 Economic analysis of recovery process.

Open Access Article. Published on 23 December 2020. Downloaded on 3/29/2026 8:09:53 AM.
This article is licensed under a Creative Commons Attribution-NonCommercial 3.0 Unported Licence.

product is Li_2CO_3 and there are few other peaks, which indicates that the purity of the precipitated product is very high.

3.6 Recovery process analysis and economic analysis

The contents of Mn, Ni, Co and Li in the leachate during separation process were shown in Table S3.† As shown in Table S3,† the valuable metals were separated efficiently and the precipitation rates of Mn, Ni, Co, and Li reached 99.5%, 99.6%, 99.2%, and 90% under the optimal conditions. Mn_xO_y, $C_8H_{14}N_4NiO_4$, $Co(OH)_2$ and Li_2CO_3 can be used in industrial production or in the resynthesize of cathode materials after simple further purification, such as ion exchange.[37] The filtrate (mainly sulfate solution) produced after recovery can be recycled.

Fig. 10 shows the material balance, energy balance and waste management in the whole process of recovering 100 g disassembled products. The currency used in this economic analysis is US dollars. The precipitation products of Ni were further treated by sulfuric acid and sodium hydroxide. It can be found that the cost of NaOH ($0.236), DMG ($C_4H_8N_2O_2$, $0.115), $(NH_4)_2S_2O_8$ ($0.111) are the highest. There are four kinds of energy consumption of various experimental operations in the whole process, the total energy consumption is $0.183. Finally, it can be found that the waste generated in the recycling process is very small, and the corresponding total cost of waste treatment is $0.004. About $0.927 can be earned by corresponding products of valuable metals. Therefore, the total profit of recycling 100 g disassembled products should be $0.141.

The recovery process has the following characteristics: (1) the precipitant used in this process has high selectivity, which can avoid the occurrence of co-precipitation to the greatest extent. (2) During the process, the pH changes from low to high throughout the process, which avoids back and forth adjustment of the pH, saves the number of acid–base reagents, and simplifies operations. (3) The mechanical disassembly of the mixed spent LIBs has the characteristics of high efficiency and safety, and the mechanical disassembly device is closed cycle without waste gas releasing.

4. Conclusions

In this paper, a novel recovery process was used to recover valuable metals from the leachate of the mechanically disassembled products. Ni, Co, Mn, Li can be effectively recovered by multi-step directional precipitation. Firstly, Mn^{2+} was oxidized to form Mn_xO_y by $(NH_4)_2S_2O_8$ on optimal conditions of pH = 5.5, temperature 80 °C, 90 min, MRNM = 3, under which about 99.5% of Mn^{2+} was recovered. Then, DMG was used to selectively precipitate Ni^{2+}. Under the optimal conditions of pH = 6, 30 °C, MRCN = 2, and 20 min, about 99.6% Ni^{2+} can be recovered. The relatively pure $C_8H_{14}N_4NiO_4$ was obtained. NaOH was used to adjust the equilibrium pH of the filtrate to 10, and at 30 °C for 15 min, about 99.2% of Co^{2+} could be recovered. Finally, Li^+ was precipitated with Na_2CO_3, which about 90% of Li was recovered. The process is efficient, economical and easily for especially suitable for the large-scale processing of mixed spent LIBs, which has great potential for industrial application.

Conflicts of interest

There are no conflicts to declare.

Acknowledgements

Financial support from National Key Research and Development Program of China (2019YFC1907900) the National Natural Science Foundation of China (51764029, 52004116), the National Key Research and Development Program of China (2019YFC1803501), the Science Research Foundation of Yunnan Provincial Department of Education (2020J0070), the Applied Basic Research Plan of Yunnan Province (202001AU070039, 2018FB087), the High-level Talent Introduction Scientific Research Start Project of KUST (20190015) and the Science and Technology Plan of Shenzhen (JSGG20180508154602283).

References

1 G. Harper, R. Sommerville, E. Kendrick, L. Driscoll, P. Slater, R. Stolkin, A. Walton, P. Christensen, O. Heidrich, S. Lambert, A. Abbott, K. S. Ryder, L. Gaines and P. Anderson, *Nature*, 2019, **575**, 75–86.
2 X. Zhang, L. Li, E. Fan, Q. Xue, Y. Bian, F. Wu and R. Chen, *Chem. Soc. Rev.*, 2018, **47**, 7239–7302.
3 W. Wang, Y. Zhang, X. Liu and S. Xu, *ACS Sustainable Chem. Eng.*, 2019, **7**, 12222–12230.
4 Y. Yang, S. Lei, S. Song, W. Sun and L. Wang, *Waste Manage.*, 2020, **102**, 131–138.
5 X. Yang, P. Dong, T. Hao, Y. Zhang, Q. Meng, Q. Li and S. Zhou, *Jom*, 2020, **72**, 3843–3852.
6 S. Zhou, Y. Zhang, Q. Meng, P. Dong, Z. Fei and Q. Li, *J. Environ. Manage.*, 2021, **277**, 111426.
7 Q. Li, K. Y. Fung and K. M. Ng, *ACS Sustainable Chem. Eng.*, 2019, **7**, 12718–12725.
8 Q. Meng, Y. J. Zhang and P. Dong, *J. Cleaner Prod.*, 2018, **180**, 64–70.
9 X. Chen, D. Kang, L. Cao, J. Li, T. Zhou and H. Ma, *Sep. Purif. Technol.*, 2019, **210**, 690–697.
10 D. Dutta, A. Kumari, R. Panda, S. Jha, D. Gupta, S. Goel and M. K. Jha, *Sep. Purif. Technol.*, 2018, **200**, 327–334.
11 C. Hanisch, T. Loellhoeffel, J. Diekmann, K. J. Markley, W. Haselrieder and A. Kwade, *J. Cleaner Prod.*, 2015, **108**, 301–311.
12 W. S. Fonseca, X. Meng and D. Deng, *ACS Sustainable Chem. Eng.*, 2015, **3**, 2153–2159.
13 H. Nie, L. Xu, D. Song, J. Song, X. Shi, X. Wang, L. Zhang and Z. Yuan, *Green Chem.*, 2015, **17**, 1276–1280.
14 M. Sathiya, A. Prakash, K. Ramesha and A. Shukla, *Mater. Res. Bull.*, 2009, **44**, 1990–1994.
15 Q. Sa, E. Gratz, M. He, W. Lu, D. Apelian and Y. Wang, *J. Power Sources*, 2015, **282**, 140–145.

 © 2021 The Author(s). Published by the Royal Society of Chemistry

Open Access Article. Published on 23 December 2020. Downloaded on 3/29/2026 8:09:53 AM.
This article is licensed under a Creative Commons Attribution-NonCommercial 3.0 Unported Licence.

16 Y. Liu, M. Zhang, Y. Xia, B. Qiu, Z. Liu and X. Li, *J. Power Sources*, 2014, **256**, 66–71.
17 T. Georgi-Maschler, B. Friedrich, R. Weyhe, H. Heegn and M. Rutz, *J. Power Sources*, 2012, **207**, 173–182.
18 J. Nan, D. Han and X. Zuo, *J. Power Sources*, 2005, **152**, 278–284.
19 D. A. Bertuol, C. M. Machado, M. L. Silva, C. O. Calgaro, G. L. Dotto and E. H. Tanabe, *Waste Manag.*, 2016, **51**, 245–251.
20 R. Zheng, L. Zhao, W. Wang, Y. Liu, Q. Ma, D. Mu, R. Li and C. Dai, *RSC Adv.*, 2016, **6**, 43613–43625.
21 P. Meshram, B. Pandey and T. Mankhand, *Chem. Eng. J.*, 2015, **281**, 418–427.
22 L.-P. He, S.-Y. Sun, Y.-Y. Mu, X.-F. Song and J.-G. Yu, *ACS Sustainable Chem. Eng.*, 2016, **5**, 714–721.
23 H. Ku, Y. Jung, M. Jo, S. Park, S. Kim, D. Yang, K. Rhee, E.-M. An, J. Sohn and K. Kwon, *J. Hazard. Mater.*, 2016, **313**, 138–146.
24 X. Zeng, J. Li and B. Shen, *J. Hazard. Mater.*, 2015, **295**, 112–118.
25 Q. Meng, Y. J. Zhang and P. Dong, *Waste Manage.*, 2017, **64**, 214–218.
26 R.-C. Wang, Y.-C. Lin and S.-H. Wu, *Hydrometallurgy*, 2009, **99**, 194–201.
27 L. Li, J. Lu, Y. Ren, X. X. Zhang, R. J. Chen, F. Wu and K. Amine, *J. Power Sources*, 2012, **218**, 21–27.
28 W. Lv, Z. Wang, H. Cao, X. Zheng, W. Jin, Y. Zhang and Z. Sun, *Waste Manag.*, 2018, **79**, 545–553.
29 D. A. Ferreira, L. M. Z. Prados, D. Majuste and M. B. Mansur, *J. Power Sources*, 2009, **187**, 238–246.
30 J. Kang, G. Senanayake, J. Sohn and S. M. Shin, *Hydrometallurgy*, 2010, **100**, 168–171.
31 G. Dorella and M. B. Mansur, *J. Power Sources*, 2007, **170**, 210–215.
32 F. Wang, R. Sun, J. Xu, Z. Chen and M. Kang, *RSC Adv.*, 2016, **6**, 85303–85311.
33 A. K. Jha, M. K. Jha, A. Kumari, S. K. Sahu, V. Kumar and B. D. Pandey, *Sep. Purif. Technol.*, 2013, **104**, 160–166.
34 T. Suzuki, T. Nakamura, Y. Inoue, M. Niinae and J. Shibata, *Sep. Purif. Technol.*, 2012, **98**, 396–401.
35 S. Barik, G. Prabaharan and B. Kumar, *Waste Manag.*, 2016, **51**, 222–226.
36 M. Rath, L. P. Behera, B. Dash, A. R. Sheik and K. Sanjay, *Hydrometallurgy*, 2018, **176**, 229–234.
37 E. Pehlivan and T. Altun, *J. Hazard. Mater.*, 2007, **140**, 299–307.